Global modes with multiple saddle points

Benoît Pier, Nigel Peake

European Journal of Mechanics B/Fluids 49 (2015) 335–344

Contents lists available at ScienceDirect

European Journal of Mechanics B/Fluids

journal homepage: www.elsevier.com/locate/ejmflu

Global modes with multiple saddle points

Benoît Pier [a,*], Nigel Peake [b]

[a] Laboratoire de mécanique des fluides et d'acoustique, École centrale de Lyon — CNRS — Université de Lyon 1 — INSA Lyon, 36 avenue Guy-de-Collongue, 69134 Écully, France

[b] Department of Applied Mathematics and Theoretical Physics, Center for Mathematical Sciences, University of Cambridge, Wilberforce Road, Cambridge CB3 0WA, UK

ARTICLE INFO

Article history:
Available online 3 April 2014

Keywords:
Absolute instabilities
Global modes
Complex saddle points

ABSTRACT

Significant progress has been made towards understanding the global stability of slowly-developing shear flows. The WKBJ theory developed by Patrick Huerre and his co-authors has proved absolutely central, with the result that both the linear and the nonlinear stability of a wide range of flows can now be understood in terms of their local absolute/convective instability properties. In many situations, the local absolute frequency possesses a single dominant saddle point in complex X-space (where X is the slow streamwise coordinate of the base flow), which then acts as a single wavemaker driving the entire global linear dynamics. In this paper we consider the more complicated case in which multiple saddles may act as the wavemaker for different values of some control parameter. We derive a frequency selection criterion in the general case, which is then validated against numerical results for the linearized third-order Ginzburg–Landau equation (which possesses two saddle points). We believe that this theory may be relevant to a number of flows, including the boundary layer on a rotating disk and the eccentric Taylor–Couette–Poiseuille flow.

1. Introduction

Over the last twenty to thirty years, the investigation of the long-time response of a shear flow to impulsive forcing has become one of the most active areas of fluid mechanics research. In these developments Patrick Huerre has played a huge and seminal role.

In the parallel-flow case, the theory of [1,2] leads to the distinction between convective instability, in which disturbances grow at the same time as being swept out of the system, and absolute instability, in which an unstable Fourier mode with zero group velocity grows *in situ* and eventually dominates the whole fluid domain. This theory has been successfully applied to a wide range of flows which exhibit a transition from convective to absolute instability as some control parameter is varied, including plane mixing layers [3], heated jets [4], and the boundary layer on a rotating disk [5,6].

For non-parallel flow, much attention has focused on the case in which the base flow evolves only slowly in space, allowing the separation of scales between slow, X, and fast, x, streamwise coordinates. We then have the concept of local convective and absolute instability, in which the base flow at a given value of X is used to compute a local absolute frequency as if for parallel flow, $\omega_0(X)$ say. Many flows contain regions of local absolute instability, where[1] $\omega_{0,i} > 0$, and adjacent regions of local convective instability or local stability, where $\omega_{0,i} < 0$. An example of such a flow is the wake of a bluff body, as noted by [7], with a pocket of local absolute instability close to the body and a region of local convective instability downstream. The key question here, however, is how the local stability properties can be connected to the behaviour of the whole system, and in particular how one can construct from the local data a global mode, in which the whole system oscillates with the same frequency, ω_G say. A significant step forward in this regard was made by [8], who showed how ω_G is given by the saddle point of $\omega_0(X)$ in the complex X-plane: the saddle point is then the effective location of a wavemaker which drives the global oscillation of the whole flow. These ideas are presented in detail in [9,10], while applications to the wake flow in particular are given in [11,12]. Situations with more complicated branch structures have been investigated by [13]. At this point we should also mention that while the above analysis has been

* Corresponding author.
E-mail address: benoit.pier@ec-lyon.fr (B. Pier).

[1] Throughout this paper, subscripts i and r denote imaginary and real parts of a complex quantity.

http://dx.doi.org/10.1016/j.euromechflu.2014.03.006
0997-7546/

concerned with linearized unsteady flow, the same ideas also pertain in nonlinear systems. In particular, [14] shows that the global nonlinear dynamics are again driven by a wavemaker, now located close to the transition station from local convective to local absolute instability, with solutions in the two regions connected across a relatively sharp front region.

To date much of the work on the global stability of weakly non-parallel flow has concentrated on the case in which there exists just a single saddle point $\omega_0(X)$ which controls the dynamics. In terms of a simple model, this behaviour is replicated by the second-order linearized Ginzburg–Landau equation. However, there are other flows in which several saddle points are present, with the possibility of the dynamics being driven by different saddles depending on the value of some control parameter. We mention two cases here. First, [15] shows that the rotating-disk boundary layer possesses two separate branches of saddle points, which for a particular Reynolds number (equivalently a particular disk radius) collide at what is termed as a 'super branch point'. The role of these two saddle points in determining the linear global behaviour of the rotating disk remains an open question. Second, it has recently been shown [16] that the dispersion relation of the eccentric Taylor–Couette–Poiseuille flow displays several saddle points and that the absolute instability may switch between these saddles when control parameters are varied. In typical oil-drilling applications the eccentricity slowly changes with axial distance: a global stability analysis of such a configuration is thus expected to involve multiple saddle points.

In the light of the issues described in the previous paragraph, our aim in this paper is to develop a linear global mode selection criterion for problems containing multiple saddle points, and to test this criterion on the simple model problem of the linearized third-order Ginzburg–Landau equation (which possesses two saddle points). The paper is set out as follows. The problem formulation and basic theory is given in Section 2. In Section 3 we present our global frequency selection criterion, which is then applied in Section 4 to the third-order Ginzburg–Landau equation. Comparisons between our criterion and the results of a full numerical integration are presented in Section 5, and excellent agreement is found.

2. Problem formulation

Consider a system governed by a one-dimensional linear partial differential equation that is first-order in time of the form

$$\partial_t \psi = \mathcal{L}(\partial_x; X)\psi, \tag{1}$$

where x and t represent space and time coordinates, respectively. The differential operator $\mathcal{L}$ depends on the space through a slow coordinate X to be defined shortly. The basic state is assumed to be $\psi = 0$, and the complex-valued function $\psi(x, t)$ represents fluctuations riding on this basic state. Solutions to the linear governing equation (1) may be sought as a superposition of global modes of the form

$$\psi(x, t) = \phi(x; \omega) \exp(-\mathrm{i}\omega t), \tag{2}$$

where the spatial functions ϕ and the complex frequencies ω obey the eigenvalue problem

$$-\mathrm{i}\omega\phi = \mathcal{L}(\partial_x; X)\phi, \tag{3}$$

derived from (1). Many global modes are in general possible, and the medium governed by (1) is stable if $\omega_i < 0$ for all global modes or unstable if $\omega_i > 0$ for at least one global mode.

A crucial assumption of the present investigation is the slow spatial development as exemplified by the introduction of the slow spatial variable X in the operator $\mathcal{L}$. The weak non-uniformity hypothesis is fulfilled if the ratio $\epsilon = \lambda/L$ between the typical instability length scale λ and the inhomogeneity length scale L is small. As a result of this scale separation, the weak spatial variations of the medium properties are described through the slow variable

$$X = \epsilon x \quad \text{with } \epsilon \ll 1, \tag{4}$$

and the time-periodic global-mode solutions may be sought as WKBJ approximations.

Such a line of thought has been successfully implemented in situations where the entire medium is governed by a single local absolute frequency $\omega_0(X)$, with a dominant saddle point in the complex X-plane [9,10]. The purpose of the present investigation is to address more complex situations involving higher-order dispersion relations and a competition between several saddle points.

3. Theoretical analysis

3.1. Local characteristics

Under the assumption that the governing equation only depends on space through the slow variable X, local characteristics may be derived from (1) by freezing X to some arbitrary value and studying the corresponding strictly uniform system. At this local level of analysis, X and x may then be considered to be independent: the fast x is involved in spatial differentiation whereas the slow X plays the role of an independent control parameter.

Any perturbation can then be sought as a superposition of elementary waves $\mathrm{e}^{\mathrm{i}(kx-\omega t)}$ where the wavenumber k and the frequency ω satisfy the local linear dispersion relation

$$\omega = \Omega(k; X) \equiv \mathrm{i}\mathcal{L}(\mathrm{i}k; X). \tag{5}$$

This dispersion relation is assumed to be an analytic function of the complex wavenumber k and it may be thought of as a polynomial in k. (It is also assumed analytic in slow space X, but the parametric dependence in X will be ignored in this section for simplicity.) Solving (5) for a given frequency ω yields a set of spatial branches $k^n(\omega)$ indexed by n; with $n = 1, 2, \ldots, N$ in the situation where $\Omega(k)$ is an N-order polynomial in k.

By invoking causality and assuming that the temporal growth rates are bounded, the spatial branches may be labelled as either k^{n+} or k^{n-} branches according to whether they are confined to the upper or lower complex k-planes for sufficiently large imaginary parts of ω. When ω_i is lowered, branch switching occurs when two spatial branches meet at $k = k_0$ for a frequency $\omega = \omega_0$. Such a wavenumber–frequency pair is defined by the saddle criterion

$$\frac{\partial\Omega}{\partial k}(k_0) = 0 \quad \text{and} \quad \omega_0 = \Omega(k_0). \tag{6}$$

In the situation where the dispersion relation (5) is an N-th order polynomial in k, the criterion (6) yields a set of $N-1$ solutions $k = k_0^n$ $(1 \le n \le N-1)$ each associated with the corresponding frequency $\omega_0^n \equiv \Omega(k_0^n)$.

Let us assume here that the frequencies ω_0^n are sorted by decreasing imaginary part: $\omega_{0,i}^1 > \omega_{0,i}^2 > \cdots$. Then, when lowering ω_i, the first branch switching occurs for $\omega = \omega_0^1$ where two spatial branches, say $k^{n_1}(\omega)$ and $k^{n_2}(\omega)$, meet at k_0^1. If this collision is between a $+$ and a $-$ branch, *e.g.* between $k^{n_1+}(\omega)$ and $k^{n_2-}(\omega)$, it corresponds to the absolute instability of the system: absolute frequency ω_{abs} and absolute wavenumber k_{abs} are then given by

$$\omega_{abs} = \omega_0^1 \quad \text{and} \quad k_{abs} = k_0^1. \tag{7}$$

However, the branch switching at ω_0^1 may be between two branches of the same label, *i.e.*, between $k^{n_1+}(\omega)$ and $k^{n_2+}(\omega)$

or between $k^{n_1-}(\omega)$ and $k^{n_2-}(\omega)$. In that situation, the (k_0^1, ω_0^1)-saddle of the dispersion relation is not a genuine pinch point and lowering of the imaginary part of ω may be continued until, at one of the frequencies ω_0^n, say $\omega_0^{n_0}$, pinching between a k^+ and a k^- eventually occurs. In any case, this procedure unambiguously yields the absolute frequency and wave number as

$$\omega_{abs} = \omega_0^{n_0} \quad \text{and} \quad k_{abs} = k_0^{n_0}, \tag{8}$$

associated with one of the saddle points of the dispersion relation defined by (6).

The above analysis can be carried out for each X. Thus the spatial branches $k^{n\pm}(X, \omega)$ are obtained by solving the local dispersion relation (5) for a given frequency ω, while the saddle-point wavenumbers $k_0^n(X)$ and frequencies $\omega_0^n(X)$ are derived from the condition

$$\frac{\partial \Omega}{\partial k}(k_0; X) = 0 \quad \text{and} \quad \omega_0(X) = \Omega(k_0; X). \tag{9}$$

Among the frequencies $\omega_0^n(X)$, the local absolute frequency $\omega_{abs}(X)$ equals the one with largest imaginary part that corresponds to pinching between downstream and upstream spatial branches. Note that the frequencies $\omega_0^n(X)$ are analytic functions of the complex X-variable, while the local absolute frequency $\omega_{abs}(X)$ is not necessarily an analytic function of X since it may jump from one ω_0^n branch to another as X is varied.

3.2. Global modes

The long-time response of (1) can be sought as a linear superposition of *global modes* which are time-harmonic solutions of the form (2) of complex global frequency ω_G. Under the assumption of weak spatial inhomogeneity (4) and resorting to classical WKBJ approximations [17] such a global mode may be obtained as

$$\psi(x, t) \sim A(X) \exp\left(\frac{\mathrm{i}}{\epsilon}\int^X k(u; \omega_G)\mathrm{d}u - \mathrm{i}\omega_G t\right), \tag{10}$$

where the slowly-varying local wavenumber $k(X; \omega_G)$ is governed by the local dispersion relation (5), and the slowly-varying amplitude $A(X)$ can be obtained by higher-order expansions.

The boundary conditions for this eigenproblem are that the mode (10) follows an upstream k^--branch for $X \to -\infty$ and a downstream k^+-branch for $X \to +\infty$. This corresponds to the fact that the modes are self-sustained and not triggered by boundary conditions, *i.e.* their selection takes place in the central region and the waves that propagate towards $X = \pm\infty$ are the consequences of this self-sustained process. As shown by [9,10] in the context of the spatially inhomogeneous complex Ginzburg–Landau equation, the necessary connection of a k^--branch prevailing near $X = -\infty$ to a k^+-branch prevailing near $X = +\infty$ can be achieved at a saddle point of the absolute frequency in the complex X-plane. This necessarily involves a dispersion relation which is second-order in the spatial wavenumber. We will now show how to generalize this theory to the case of a higher-order dispersion relation.

In the previous section we described how the saddle point frequencies $\omega_0^n(X)$ may be defined via a local analysis of the dispersion relation for each value of X in the complex plane. Each mapping $X \mapsto \omega_0^n(X)$ is analytic and may be thought of as a polynomial of order N_n. Then there are N_n pre-images, say $\omega \mapsto X^{(n,p)}(\omega)$ for $1 \le p \le N_n$, in the complex X-plane, obtained as the inverse mapping $\left(\omega_0^n\right)^{-1}$ of a given contour in the complex ω-plane. We assume, as is standard, that the medium is stable, or at most convectively unstable, towards $X \to \pm\infty$, which means that $\max_n Im\,\omega_0^n(X)$ for X on the real axis exists. Now consider a horizontal L-contour in the complex ω-plane (see Fig. 1b), above all $\omega_0^n(X)$ for X along the real axis (M-contour). Then the associated contours $X^{(n,p)}(\omega)$ do not cross the real axis (the M-contour) for ω along the L-contour and may therefore be labelled as $X^{(n,p)+}$ or $X^{(n,p)-}$ depending on whether they are confined to the upper or lower half X-planes respectively (see Fig. 1a). When the L-contour is lowered, it approaches the $\omega_0^n(X)$ curves in the ω-plane, and the $X^{(n,p)\pm}$-curves move in closer to the M-contour in the X-plane. As the L-contour is lowered further, it may be necessary to deform the M-contour to avoid a collision with one of the X-branches, and the $\omega_0^n(X)$-curves in the ω-plane are then deformed accordingly. Eventually, however, this process cannot be continued as the M-contour gets pinched between an X^+-branch and an X^--branch (Fig. 1c); this pinching in the X-plane corresponds, in the ω-plane, to the L-contour passing through a cusp of one of the ω_0^n-curves (Fig. 1d).

The arrangement of the $\omega_0^n(X)$ and $X^{(n,p)\pm}(\omega)$ curves for X along the M-contour and ω along the L-contour is then as follows. In the complex ω-plane (Fig. 1d), the horizontal L-contour lies above all $\omega_0^n(X)$-curves and passes through a cusp at, say, ω_s^1 of the ω_0^1-curve. In the complex X-plane (Fig. 1c), the deformed M-contour is pinched at, say, X_s^1 between the curves $X^{(1,1)+}$ and $X^{(1,2)-}$. All other $\omega_0^n(X)$-curves (for $n \neq 1$) are below the L-contour in the ω-plane, and all other $X^{(n,p)+}$-curves (respectively $X^{(n,p)-}$-curves) are above (respectively below) the M-contour in the X-plane. This saddle point is characterized by X_s^1 and ω_s^1 and obeys the condition

$$\frac{d\omega_0^1}{dX}(X_s^1) = 0 \quad \text{and} \quad \omega_s^1 = \omega_0^1(X_s^1), \tag{11}$$

or equivalently

$$\frac{\partial \Omega}{\partial X}(k_s^1, X_s^1) = \frac{\partial \Omega}{\partial k}(k_s^1, X_s^1) = 0 \quad \text{and} \quad \omega_s^1 = \Omega(k_s^1, X_s^1), \tag{12}$$

where k_s^1 is the wavenumber value at which two spatial branches $k(X; \omega_s^1)$ pinch when $X = X_s^1$ along the M-contour, and no other connection between spatial branches is possible along the M-contour.

If this connection at X_s^1 is between a k^+- and a k^--branch, then a global mode of the form (10) and frequency $\omega_G = \omega_s^1$ has been found. This is the classical result. It may, however, happen that this connection is between two k^+- or between two k^--branches, which does not lead to a global mode solution. Therefore, the above saddle-point criterion in the complex X-plane yields a global mode solution only if the associated $\omega_0^1(X)$ indeed corresponds to the absolute frequency of the system for $X = X_s^1$, *i.e.*, if

$$\omega_{abs}(X_s^1) = \omega_0^1(X_s^1). \tag{13}$$

When condition (13) is not fulfilled, another saddle point must be sought to connect a k^--branch to a k^+-branch. Then, the process is continued by lowering the L-contour further in the ω-plane (except in a small region around ω_s^1). Via a similar scenario to previously, this eventually leads to a new pinching of the deformed M-contour at, say, X_s^2 between the curves $X^{(2,1)+}$ and $X^{(2,2)-}$, while the L-contour passes through a cusp at, say, ω_s^2 of the $\omega_0^2(X)$-curve (see Fig. 1e,f). This new saddle point obeys a criterion similar to (12). Again, a connection between k^+- and k^--branches has been found if the additional condition similar to (13) is met. If not, the process goes on by lowering the L-contour even further in the ω plane (except in small regions around ω_s^1 and ω_s^2) until, eventually, a saddle point associated with the local absolute frequency is found.

A systematic implementation of this strategy leads to the following criterion for the global mode frequency ω_G:

$$\omega_G = \omega_{abs}(X_s), \tag{14}$$
$$\frac{\partial \Omega}{\partial X}(k_s, X_s) = \frac{\partial \Omega}{\partial k}(k_s, X_s) = 0 \quad \text{and} \quad \Omega(k_s, X_s) = \omega_{abs}(X_s).$$

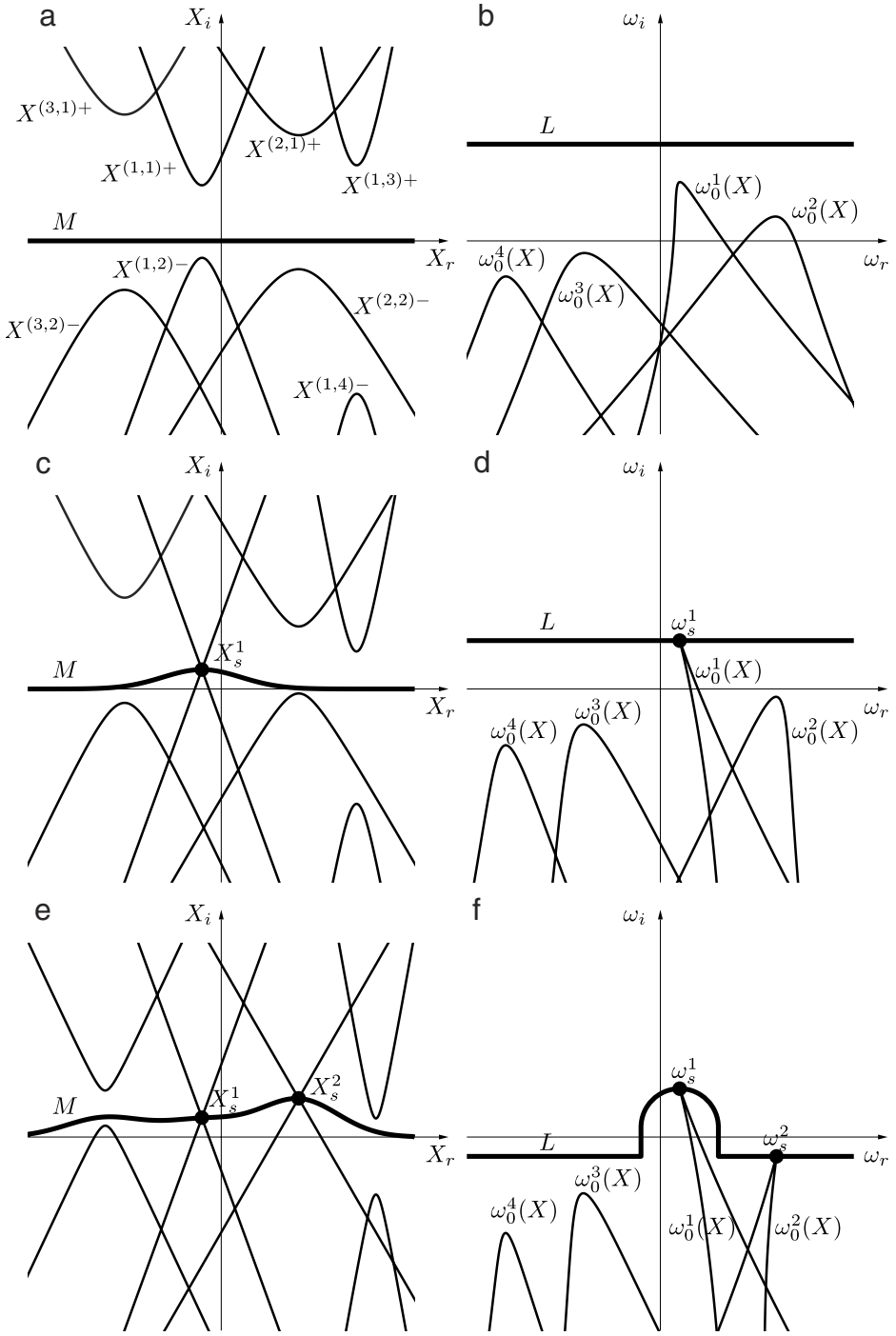

Fig. 1. (b,d,f) Loci of $\omega_0^n(X)$ in the complex ω-plane for X along corresponding M-contour in the complex X-plane. (a,c,e) Loci of $X^{(n,p)\pm}(\omega)$ in the complex X-plane for ω along corresponding L-contour in the complex ω-plane.

The subtle difference between our new criterion (14) and the classic result

$$\omega_G = \omega_{abs}(X_s) \quad \text{and} \quad \frac{d\omega_{abs}}{dX}(X_s) \tag{15}$$

lies in the fact that, in this more general case, there is no guarantee that the local absolute frequency $\omega_{abs}(X)$ is an analytic function over the entire complex plane, even if the dispersion relation $\Omega(k, X)$ is analytic in both k and X.

In the next section we will illustrate our general result by designing the simplest possible partial differential equation exhibiting a local dispersion relation with two saddle points.

4. Toy model

The requirement of more than one saddle point in the dispersion relation leads us to consider a partial differential equation with third-order spatial derivatives

$$\frac{\partial \psi}{\partial t} = a_0(X)\psi + a_1(X)\frac{\partial \psi}{\partial x} + a_2(X)\frac{\partial^2 \psi}{\partial x^2} + a_3(X)\frac{\partial^3 \psi}{\partial x^3}, \tag{16}$$

which corresponds to the dispersion relation

$$\Omega(k, X) \equiv \mathrm{i}a_0(X) - a_1(X)k - \mathrm{i}a_2(X)k^2 + a_3(X)k^3. \tag{17}$$

In the following subsections we will identify the possible choices of the complex coefficients $a_0(X), \ldots, a_3(X)$, and discuss a range

of interesting possible behaviours. Our theory will be confirmed by comparison with direct numerical simulation of (16).

4.1. Local dispersion relation

Let us first consider the *local* situation, by assuming a spatially homogeneous configuration where the coefficients $a_0, \ldots, a_3$ do not depend on X.

Causality requires that temporal growth rates are bounded above, *i.e.* $\Omega_i(k)$ is bounded above when $k \to \pm\infty$. This condition is met when a_3 is real and $a_{2,r} > 0$. Without loss of generality, we will use $a_3 = 1$ from now on, which corresponds to a rescaling of the temporal coordinate. Thus the dispersion relation is entirely determined by the three complex parameters a_0, a_1 and a_2 (with $a_{2,r} > 0$).

Since the dispersion relation is a third-order polynomial in k, there are two saddle points that satisfy $\partial_k \Omega = 0$. The frequencies and wavenumbers of these saddle points may be written as

$$\omega_0^1 = \omega_0 + \delta\omega_0 \quad \text{and} \quad k_0^1 = k_0 + \delta k_0, \tag{18}$$

$$\omega_0^2 = \omega_0 - \delta\omega_0 \quad \text{and} \quad k_0^2 = k_0 - \delta k_0. \tag{19}$$

Since only three of these four parameters are independent, the local dispersion relation may be entirely specified by the three complex parameters ω_0, k_0 and δk_0 as

$$\omega - \omega_0 = (k - k_0)^3 - 3(\delta k_0)^2 (k - k_0), \tag{20}$$

which corresponds to

$$a_0 = \mathrm{i}\left[k_0^3 - 3(\delta k_0)^2 k_0 - \omega_0\right], \tag{21}$$

$$a_1 = 3\left[(\delta k_0)^2 - k_0^2\right], \tag{22}$$

$$a_2 = -3\mathrm{i}k_0, \tag{23}$$

$$a_3 = 1. \tag{24}$$

The fourth (dependent) parameter follows as $\delta\omega_0 = -2(\delta k_0)^3$, and the causality condition $a_{2,r} > 0$ is fulfilled for $k_{0,i} > 0$.

In this section we will not consider the detailed local behaviour, in terms of local absolute/convective instability, which depends in a complicated way on the local values of the complex coefficients $a_0, \ldots, a_3$. However, in the Appendix we will derive the Green's function for the constant-coefficient third-order equation with general complex $a_0, \ldots, a_3$, which we will then use to find implicit conditions for local stability in the simplified case of real coefficients.

4.2. Local absolute frequency

The dispersion relation (20) is characterized by the two saddle points $\omega_0 \pm \delta\omega_0$ at $k_0 \pm \delta k_0$ (18) and (19), with $\delta\omega_0 = -2(\delta k_0)^3$. In order to work out which one of these saddle points yields the local absolute frequency, the method outlined in the previous section may be used.

The asymptotic behaviour of the dispersion relation (20) is that $\omega \sim k^3$ as $|k| \to \infty$. Hence, for sufficiently large $\omega_i > 0$, frequencies along a horizontal line $\omega_i = \text{const}$ in the complex ω-plane are associated with two spatial k^+-branches and one spatial k^--branch in the complex k-plane: say k^{1+}, k^{2+} and k^{3-} with $\mathrm{Arg}(k^n) \to (n-1)2\pi/3$ for $\omega_r \to \infty$.

We will now show that the choice of the local absolute frequency, i.e. $\omega_{abs} = \omega_0^1$ or $\omega_{abs} = \omega_0^2$, only depends on the value of δk_0. We write $\delta k_0 = \kappa \mathrm{e}^{\mathrm{i}\phi}$ with $\kappa > 0$, so that $\delta\omega_0 = 2\kappa^3 \mathrm{e}^{\mathrm{i}(3\phi+\pi)}$, and consider the different ranges of values of ϕ as follows:

(i) First consider the case $0 < \phi < \pi/3$, which gives $\omega_{0,i}^1 < \omega_{0,i}^2$. When lowering the horizontal line $\omega_i = \text{const}$ in the complex ω-plane, the first saddle-point frequency to be crossed is $\omega_0^2 \equiv \omega_0 - \delta\omega_0$ (see Fig. 2a). For $\omega = \omega_0^2$, two spatial branches meet at $k_0^2 \equiv k_0 - \delta k_0$. Since $\pi < \mathrm{Arg}(-\delta k_0) < 4\pi/3$, the pinch at k_0^2 is between the k^{3-} and the k^{2+} branches (see Fig. 2b). Therefore, $\omega_{abs} = \omega_0^2$ and $k_{abs} = k_0^2$, in this case.

(ii) Next consider the case $\pi/3 < \phi < 2\pi/3$, which corresponds to $\omega_{0,i}^2 < \omega_{0,i}^1$. When lowering the horizontal line $\omega_i = \text{const}$ in the complex ω-plane, the first saddle-point frequency to be crossed is ω_0^1 (see Fig. 2c). For $\omega = \omega_0^1$, two spatial branches meet at $k_0^1 \equiv k_0 + \delta k_0$. Since $\pi/3 < \mathrm{Arg}(+\delta k_0) < 2\pi/3$, the saddle at k_0^1 is between the k^{1+} and k^{2+} branches (see Fig. 2d). Thus, the (k_0^1, ω_0^1)-saddle does not yield the absolute frequency of the system, and the lowering of the contour $\omega_i = \text{const}$ may be continued until ω_0^2 is reached. For $\omega = \omega_0^2$, two spatial branches meet at $k_0^2 \equiv k_0 - \delta k_0$. The pinch at k_0^2 is between the k^{3-}-branch and a branch that results from the recombination of the two k^+-branches. Therefore, one has again that $\omega_{abs} = \omega_0^2$ and $k_{abs} = k_0^2$.

(iii) The case $2\pi/3 < \phi < \pi$ is similar to the case $0 < \phi < \pi/3$, and yields $\omega_{abs} = \omega_0^2$ and $k_{abs} = k_0^2$ by pinching of k^{1+} and k^{3-}.

(iv) Analysing in turn the three remaining cases $\pi < \phi < 4\pi/3$, $4\pi/3 < \phi < 5\pi/3$ and $5\pi/3 < \phi < 2\pi$, it can be shown that they all yield $\omega_{abs} = \omega_0^1$ and $k_{abs} = k_0^1$.

In summary, for dispersion relation (20) the absolute frequency is obtained by the following criterion:

$$\omega_{abs} = \omega_0^1 \quad \text{when } \delta k_{0,i} < 0, \tag{25}$$

$$\omega_{abs} = \omega_0^2 \quad \text{when } \delta k_{0,i} > 0. \tag{26}$$

Note also that the absolute frequency is the saddle-point frequency of larger imaginary part, unless $\pi/3 < \mathrm{Arg}(\delta k_0) < 2\pi/3$ or $4\pi/3 < \mathrm{Arg}(\delta k_0) < 5\pi/3$ (in which cases the saddle point corresponding to the saddle-point frequency with larger imaginary part is not a pinch point).

4.3. Global modes

For weakly inhomogeneous systems, the coefficients of the governing Eq. (16) depend on the slow spatial variable X. As shown in the previous section, the selection criterion of self-sustained global-mode solutions is based on the double saddle-point criterion (14) in the complex k- and X-planes for the local dispersion relation. We will now further specify the spatial variation of the coefficients (21)–(24) so as to check this criterion for different situations.

For the application of the spatial saddle-point criterion it is convenient to use

$$\omega_0^1(X) = \omega_s^1 + \frac{1}{2}\omega_{s,XX}^1 \left(X - X_s^1\right)^2, \tag{27}$$

$$\omega_0^2(X) = \omega_s^2 + \frac{1}{2}\omega_{s,XX}^2 \left(X - X_s^2\right)^2, \tag{28}$$

so that each of $\omega_0^{1,2}(X)$ displays exactly one saddle point at $X_s^{1,2}$ with frequency $\omega_s^{1,2}$. The use of second-order polynomials in X for $\omega_0^{1,2}(X)$ guarantees that the associated $\omega_0(X)$ and $\delta\omega_0(X)$ are also second-order polynomials.

After specifying the frequencies (27) and (28), the spatial distribution of $\delta k_0(X)$ follows from $\delta\omega_0(X) = -2[\delta k_0(X)]^3$, and so evaluation of $\delta k_0(X)$ involves a third-order root. Since $\delta\omega_0(X)$ is a second-order polynomial in X, it displays two zeroes in the complex X-plane, which correspond to two branch points for

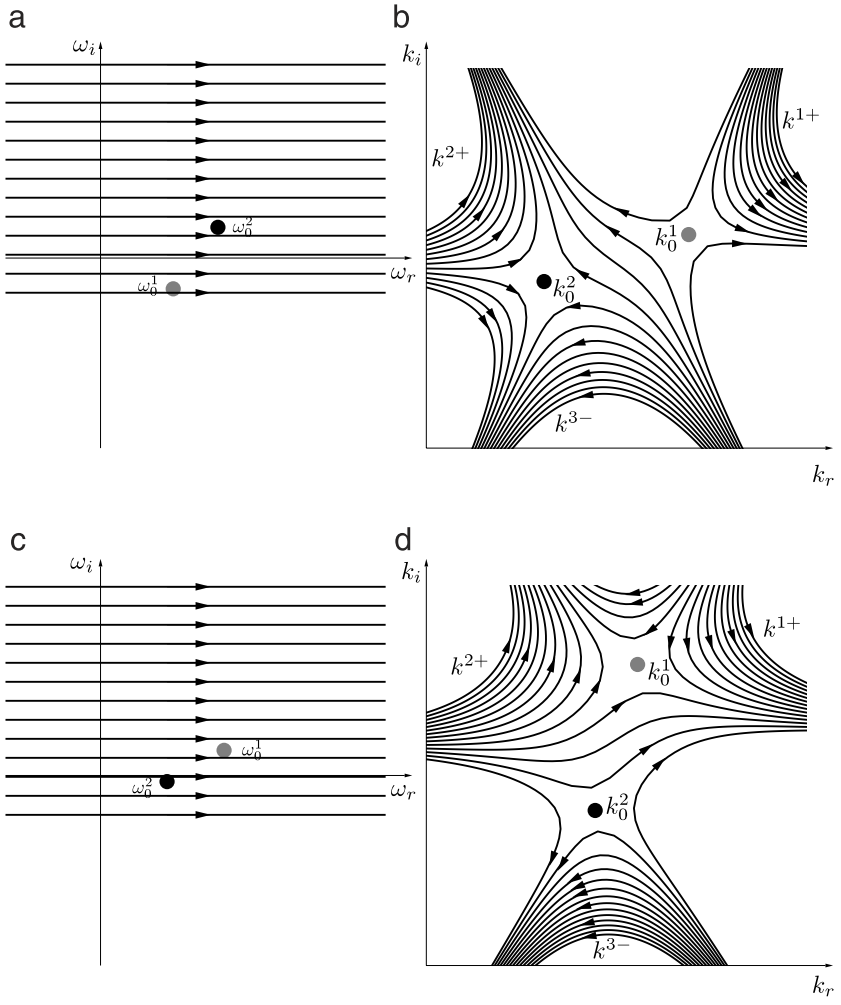

Fig. 2. Temporal branches in complex frequency plane (a,c) and spatial branches in complex wavenumber plane (b,d) for local third-order dispersion relation. (a,b) Configuration with $0 < \mathrm{Arg}(\delta k_0) < \pi/3$, (c,d) with $\pi/3 < \mathrm{Arg}(\delta k_0) < 2\pi/3$.

$\delta k_0(X)$. After choosing the associated branch cuts to lie away from the real X-axis, Eqs. (27) and (28) completely specify the three possible analytic distributions of $\delta k_0(X)$ along the real X-axis, and, for simplicity, the remaining unspecified parameter $k_0(X)$ will be chosen to be a constant in this study.

Tackling the problem the other way round, *i.e.*, by specifying an analytic distribution of $\delta k_0(X)$, would have led to complicated expressions for $\omega_0^{1,2}(X)$, preventing the closed-form determination of saddle points in the complex X-plane. Thus the introduction of a third-order root for $\delta k_0(X)$ seems a small price to pay to retain the simplest possible model. It would have been even more complicated to have started by writing down analytic expressions for the coefficients $a_0(X), \ldots, a_3(X)$, and we therefore assert that our approach of starting with quadratic expressions for $\omega_0^{1,2}(X)$ is the best way to understand the behaviour of our system.

So in summary, we have ended up with a particular class of spatially inhomogeneous system (16) that is entirely determined by the seven complex parameters

$$\omega_s^1, \omega_s^2, X_s^1, X_s^2, \omega_{s,XX}^1, \omega_{s,XX}^2 \quad \text{and} \quad k_0, \tag{29}$$

and by the additional choice of one among the three possible $\delta k_0(X)$-branches. Causality requires that $k_{0,i} > 0$, and the conditions $Im\,\omega_{s,XX}^{1,2} < 0$ prevent the medium from being locally absolutely unstable when $X_r \to \pm\infty$. The method outlined in the previous subsection and based on $\mathrm{Arg}(\delta k_0(X))$ is then used to determine the different regions of the complex X-plane where the local absolute frequency $\omega_{abs}(X)$ equals either $\omega_0^1(X)$ or $\omega_0^2(X)$. Then, according to the theoretical result (14), the frequencies ω_s^1 and ω_s^2 are possible global mode frequencies if $\omega_s^1 = \omega_{abs}(X_s^1)$ or $\omega_s^2 = \omega_{abs}(X_s^2)$. If both are possible, the mode of larger growth rate is expected to dominate in the long term. In the next section we will confirm these results by comparison with direct numerical simulation.

5. Numerical confirmation

In order to confirm the theoretical results of Section 3, direct numerical simulations of the third-order partial differential equation discussed in Section 4 were carried out for a variety of parameter settings.

The simulations presented below were performed with saddle point frequencies $\omega_0^{1,2}(X)$ determined by

$$\omega_s^1 = 1 + \mathrm{i}, \qquad X_s^1 = -\mathrm{i}, \qquad \omega_{s,XX}^1 = -0.02 - 0.10\mathrm{i}, \tag{30}$$

and

$$\omega_s^2 = 2, \qquad X_s^2 = -2 + \mathrm{i}, \qquad \omega_{s,XX}^2 = -0.05\mathrm{i}. \tag{31}$$

Using $k_0 = \mathrm{i}$, each of the three possible $\delta k_0(X)$-branches was investigated.

Fig. 3 shows isolines of $\omega_{0,i}^{1,2}(X)$ in the complex X-plane. For this configuration, the branch points of $\delta k_0(X)$ (where $\omega_0^1(X) =$

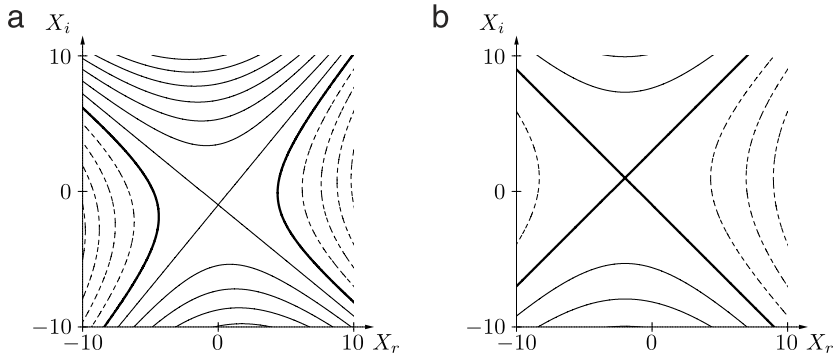

Fig. 3. Isolines of (a) $\omega_{0,i}^1$ and (b) $\omega_{0,i}^2$ in the complex X-plane. Thick line: $\omega_{0,i} = 0$, thin solid lines: $\omega_{0,i} = 1, 2, \ldots$, thin dashed lines: $\omega_{0,i} = -1, -2, \ldots$.

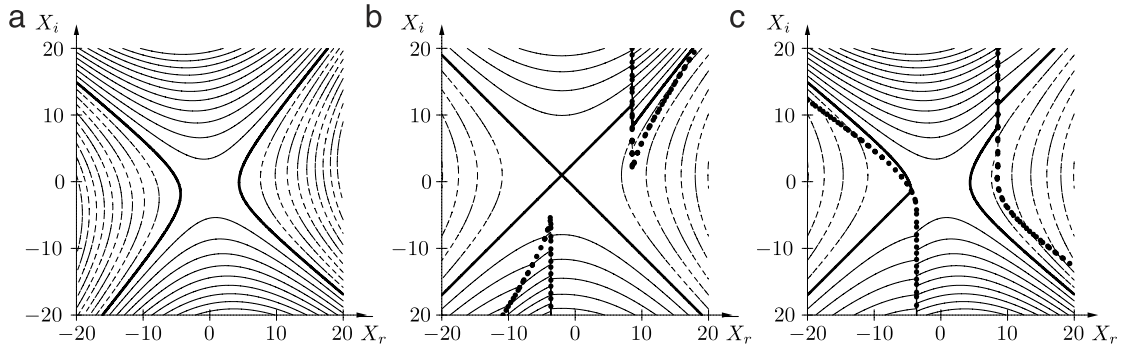

Fig. 4. Isolines of $\omega_{abs,i}(X)$ for (a) branch A, (b) branch B and (c) branch C. Thick line: $\omega_{0,i} = 0$, thin solid lines: $\omega_{0,i} = 2, 4, \ldots$, thin dashed lines: $\omega_{0,i} = -2, -4, \ldots$. Thick dotted curve represents boundary where the local absolute frequency $\omega_{abs}(X)$ switches between $\omega_0^1(X)$ and $\omega_0^2(X)$.

$\omega_0^2(X)$) are located at $X \simeq 8.51 + 0.95\mathrm{i}$ and $X \simeq -3.68 - 5.02\mathrm{i}$. Upon choosing the associated branch cuts away from the real X-axis, there are three possible choices for $\delta k_0(X)$ along the real axis (hereafter called branches A, B and C). For each case, the resulting local absolute frequency $\omega_{abs}(X)$ is illustrated by isolines of its imaginary part in the complex X-plane in Fig. 4.

For branch A, it is seen in Fig. 4(a) that $\omega_{abs}(X) = \omega_0^1(X)$ in the entire domain although ω_0^1 is the dominant saddle only in the central region. In this situation, the expected global mode frequency is therefore ω_s^1.

For branch B (Fig. 4b), the local absolute frequency $\omega_{abs}(X)$ is seen to follow $\omega_0^2(X)$ over a large domain including the real X-axis and both saddles X_s^1 and X_s^2. It is only in the two wedge-shape regions, starting at the two branch points, that the local absolute frequency equals $\omega_0^1(X)$. The expected global mode frequency is therefore ω_s^2.

For branch C (Fig. 4c), it is seen that the complex X-plane is partitioned into three regions: $\omega_{abs}(X)$ follows $\omega_0^1(X)$ in the central region and $\omega_0^2(X)$ in the regions extending towards $X = \pm\infty$. Since $\omega_{abs}(X_s^1) = \omega_s^1$, the expected global mode frequency is ω_s^1 in this configuration.

A numerical simulation of (16) performed with coefficient settings corresponding to branch A leads to the global mode shown in Fig. 5(a). Here, the inhomogeneity parameter (4) was chosen as $\epsilon = 0.1$; therefore the interval $-100 < x < 50$ corresponds to $-10 < X < 5$. The numerically determined global frequency $\omega_G = 0.98 + 0.97\mathrm{i}$ is very close to the expected $\omega_s^1 = 1 + \mathrm{i}$. Numerically, the local wavenumber is computed as $-\mathrm{i}\partial_x\psi/\psi$, and its real and imaginary parts are plotted as thick dashed lines in Fig. 5(b) and (c) respectively. The three analytical spatial branches associated with the frequency ω_s^1 are shown by thin lines in the same plots. It is seen that the local wavenumber obtained by direct numerical simulation very closely follows the expected analytical branches. The imaginary parts of $\omega_{abs}(X)$, $\omega_0^1(X)$ and $\omega_0^2(X)$ along the real X-axis are plotted in Fig. 5(d).

Numerical results corresponding to branch B are shown in Fig. 6. The mode plotted in Fig. 6(a) is synchronized to a global frequency $\omega_G = 2.01 - 0.02\mathrm{i}$, in close agreement with the expected $\omega_s^2 = 2$. Its numerically derived local wavenumber follows the associated analytical branches, as shown in Fig. 6(b,c). For this configuration, the local absolute frequency follows $\omega_0^2(X)$ over the entire real X-axis, see Fig. 6(d).

Numerical results corresponding to branch C are shown in Fig. 7. The mode plotted in Fig. 7(a) is synchronized to a global frequency $\omega_G = 1.01 + 0.98\mathrm{i}$, again in close agreement with the expected $\omega_s^1 = 1 + \mathrm{i}$. Its numerically derived local wavenumber follows the associated analytical branches, as shown in Fig. 7(b,c). For this configuration, the local absolute frequency switches between $\omega_0^1(X)$ and $\omega_0^2(X)$ along the real X-axis, as shown in Fig. 7(d).

In order to study the influence of the inhomogeneity parameter, simulations were carried out for a range of ϵ-values, while keeping the same dependence of the complex coefficients $a_n(X)$ on the slow spatial variable $X = \epsilon x$. Reducing ϵ while keeping the same X-interval thus corresponds to simulations over larger x-intervals. For all three configurations, Table 1 indicates the numerically obtained global mode frequencies ω_G as a function of ϵ and demonstrates that they nicely converge to the theoretical value as $\epsilon \to 0$.

Finally, results are presented for a configuration where the global frequency is determined by ω_s^2, while the local absolute frequency is largely dominated by $\omega_0^1(X)$. Using $\omega_s^1 = 0.5 + \mathrm{i}, X_s^1 = 10 - 8\mathrm{i}, \omega_{s,XX}^1 = -0.02 - 0.10\mathrm{i}, \omega_s^2 = 1 + 2\mathrm{i}, X_s^2 = -5, \omega_{s,XX}^2 = 0.02 - 0.05\mathrm{i}$ and $k_0 = \mathrm{i}$, the absolute frequency distribution shown in Fig. 8 is obtained. The saddle X_s^1 lies within the region where $\omega_{abs}(X) = \omega_0^1(X)$ and the X_s^2 lies within the region where $\omega_{abs}(X) = \omega_0^2(X)$. Since $\omega_{s,i}^2 > \omega_{s,i}^1$, the theory predicts a dominant global mode of frequency $\omega_G \simeq \omega_s^2 = 1 + 2\mathrm{i}$. Plotting the local

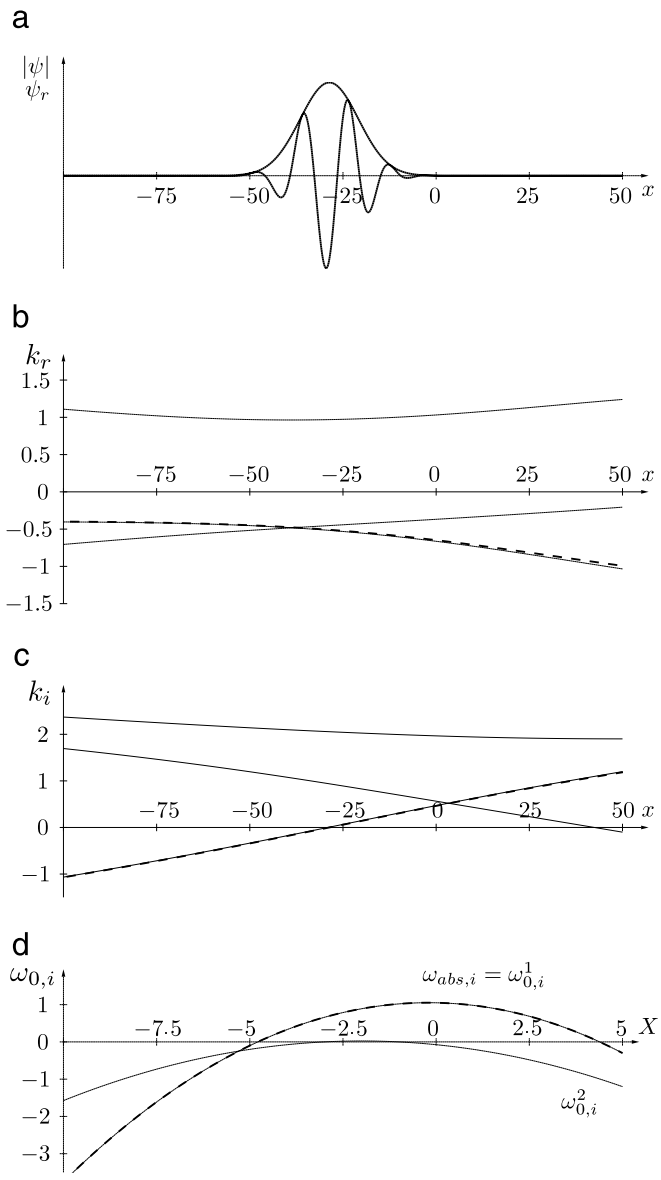

Fig. 5. Structure of global mode obtained by direct numerical simulations for configuration A. (a) Envelope $|\psi|$ and real part ψ_r as functions of streamwise distance. (b) Real part of analytically computed spatial branches (thin lines) together with local wavenumber of simulation (thick dashed line). (c) Imaginary part of analytically computed spatial branches together with local wavenumber of simulation. (d) Imaginary parts of $\omega_{abs}(X)$ (thick dashed line), together with $\omega_0^{1,2}(X)$ (thin lines).

Table 1
Dependence of numerically obtained global mode frequency ω_G on inhomogeneity parameter ϵ.

ϵ	Branch A	Branch B	Branch C
1.0	$0.818 + 0.683$i	$2.133 - 0.217$i	$1.125 + 0.754$i
0.5	$0.924 + 0.833$i	$2.064 - 0.108$i	$1.059 + 0.878$i
0.2	$0.969 + 0.934$i	$2.026 - 0.042$i	$1.025 + 0.952$i
0.1	$0.984 + 0.967$i	$2.013 - 0.021$i	$1.013 + 0.977$i
0.05	$0.992 + 0.984$i	$2.007 - 0.011$i	$1.007 + 0.990$i
0.02	$0.997 + 0.994$i	$2.003 - 0.004$i	$1.003 + 0.998$i
ω_s	$1 +$ i	2	$1 +$ i

absolute growth rate along the real X-axis (Fig. 8b) shows that the absolute instability of this system is largely dominated by the ω_0^1-branch. Nevertheless, a direct numerical simulation confirms that a global mode of frequency $\omega_G \simeq 0.92 + 1.97$i is indeed selected in this configuration (with $\epsilon = 0.2$).

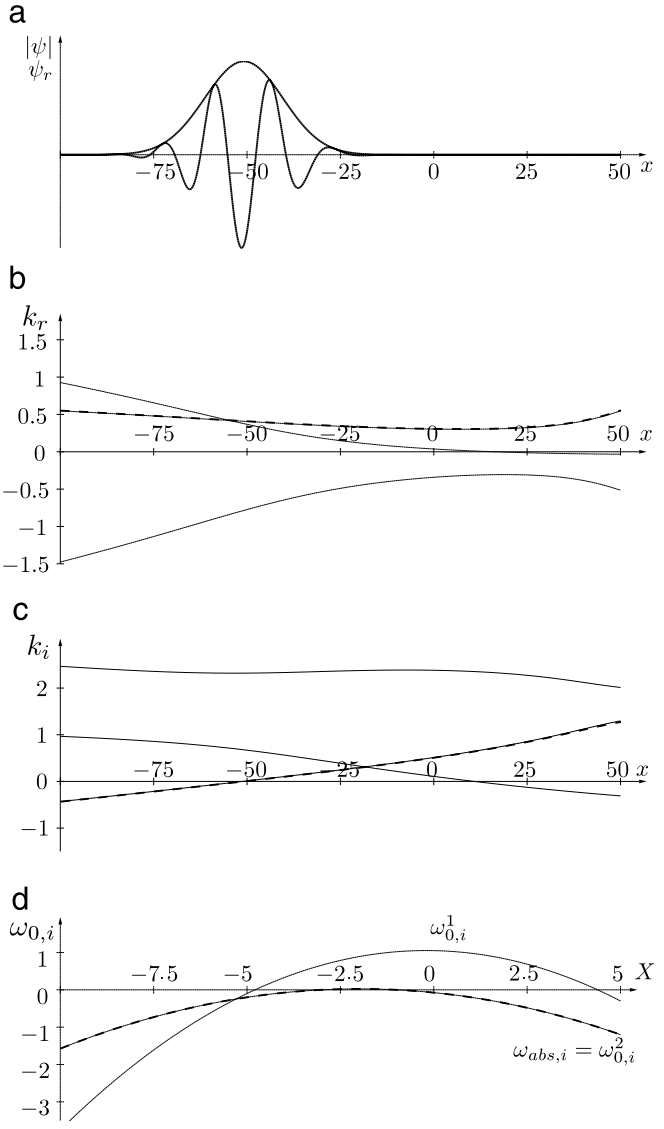

Fig. 6. Same as Fig. 5, using coefficient settings corresponding to branch B.

6. Concluding remarks

In this paper we have developed a global frequency selection criterion, Eq. (14), for weakly non-parallel systems whose local dynamics are controlled by more than one pinch point. Our result differs from the classical condition (*e.g.* [8]) in that when more than one pinch point must be considered the local absolute frequency, $\omega_{abs}(X)$, is no longer necessarily an analytic function. Of course, our condition has been derived within the context of asymptotically slow variation of the base flow ($\epsilon \to 0$), whereas in practice ϵ will be small, but nonzero. For the third-order linearized Ginzburg–Landau equation we have therefore compared our criterion with a full numerical solution, and excellent agreement has been obtained for small ϵ (and qualitative agreement even for $\epsilon = 1$).

There are a number of possibilities for further investigation. First, our criterion can be applied to a range of fluid flows, including the rotating-disk boundary layer and the eccentric Taylor–Couette–Poiseuille, as mentioned in the introduction. Second, interesting questions arise about the behaviour of the equivalent signalling problem, in which waves emitted by a fixed-frequency source propagate through the spatially-developing medium. [18] has shown that for the case of a single X-saddle (second-order Ginzburg–Landau) the system response depends on the size of the

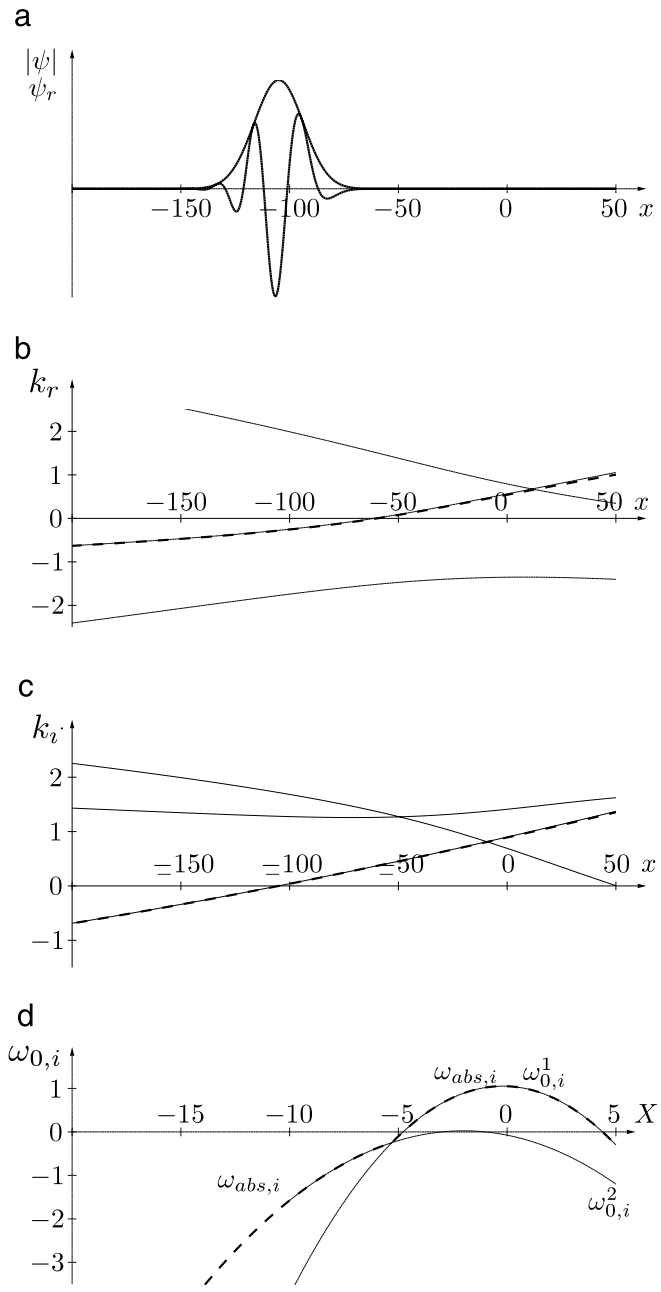

Fig. 7. Same as Fig. 5, using coefficient settings corresponding to branch C.

forcing frequency relative to the marginal frequencies at either end of the single region (if it exists) of local absolute instability. As soon as more than one saddle is present, even richer dynamics are presumably possible. Third, nonlinear analysis in the style of [19] could also be considered. In the nonlinear case, the dynamics are controlled by the local absolute frequency on the real X-axis, but again richer behaviour is presumably possible when multiple regions of local absolute instability are present, especially when those regions become closely spaced relative to the spatial extent of the nonlinear global modes.

It is a great pleasure to dedicate this article to Professor Patrick Huerre. Patrick's contribution to fluid mechanics and to the fluid mechanics community has been, and continues to be, enormous. In particular, his work on hydrodynamic instability theory has shaped the development of the subject for a generation. We also wish to record our gratitude to Patrick for his great personal kindness to us, stretching over many years.

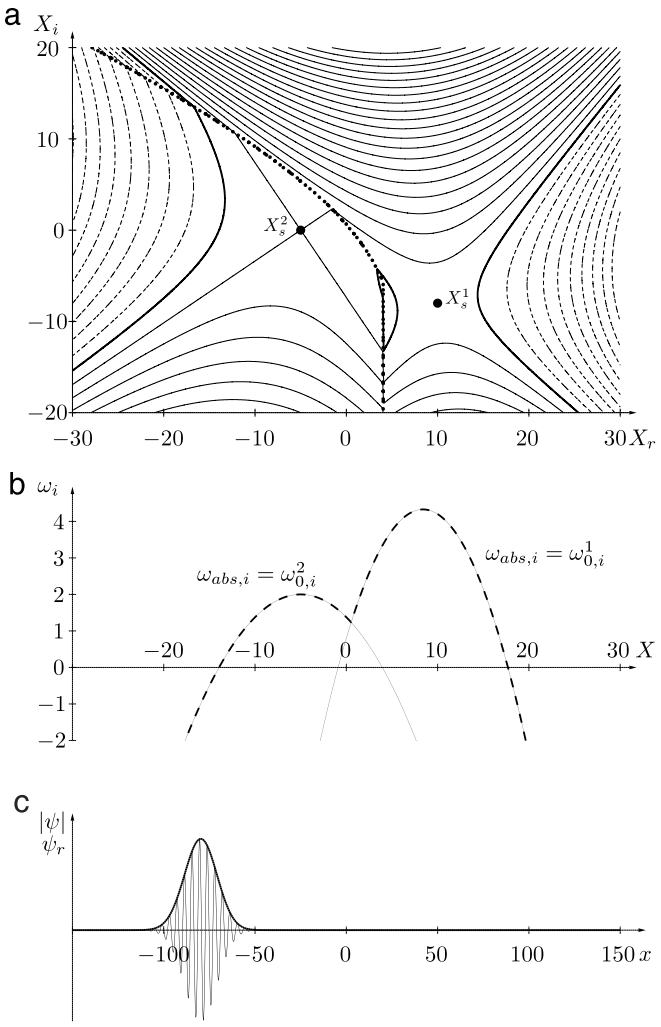

Fig. 8. (a) Isolines of local absolute growth rates in complex X-plane. Thick line: $\omega_{abs,i} = 0$, thin solid lines: $\omega_{abs,i} = 2, 4, \ldots$, thin dashed lines: $\omega_{abs,i} = -2, -4, \ldots$. Thick dotted curve represents boundary where the local absolute frequency $\omega_{abs}(X)$ switches between $\omega^1_0(X)$ and $\omega^2_0(X)$. (b) Cut along the real X-axis. (c) Structure of numerically selected global mode, for $\epsilon = 0.2$.

Appendix. Green's function

In this Appendix we will derive the Green's function of the forced constant-coefficient third-order equation

$$\frac{\partial \psi}{\partial t} = a_0\psi + a_1\frac{\partial \psi}{\partial x} + a_2\frac{\partial^2 \psi}{\partial x^2} + a_3\frac{\partial^3 \psi}{\partial x^3} + \delta(x)\delta(t). \tag{A.1}$$

We will then use the Green's function to investigate the local stability of the system.

By taking the Fourier transform of Eq. (A.1) in x, which is defined by

$$\overline{\psi}(k, t) = \int_{-\infty}^{\infty} \psi(x, t)\exp(-\mathrm{i}kx)\mathrm{d}x, \tag{A.2}$$

and noting that $\overline{\psi}(k, +0) = 1$, thanks to the presence of the $\delta(t)$ term in Eq. (A.1), it is easy to show that the Green's function is given as a Fourier inversion integral in the form

$$\psi(x, t) = \frac{\exp(a_0 t)}{2\pi}\int_{-\infty}^{\infty} \exp\left[\left(\mathrm{i}ka_1 - k^2a_2 - \mathrm{i}k^3a_3\right)t + \mathrm{i}kx\right]\mathrm{d}k. \tag{A.3}$$

In order for this integral to converge, we note that we require a_3 to be real and the real part of a_2 to be positive — these are exactly the necessary causality conditions already set out in Section 4.1.

The trick now is to complete the cube within the exponential. This is done by making the substitution $k = z + c$, for some constant c, and then choosing c so that the coefficient of z^2 within the exponential is zero. This leads to

$$\psi(x,t) = \frac{\exp(a_0 t + At)}{2\pi} \times \int_C \exp\left(\mathrm{i}z\left\{x + a_1 t - \frac{a_2^2 t}{3a_3}\right\} - \mathrm{i}a_3 t z^3\right) \mathrm{d}z, \tag{A.4}$$

where

$$A = \left(\frac{2a_2^3}{27a_3^2} - \frac{a_1 a_2}{3a_3}\right) - \frac{a_2 x}{3a_3 t}, \tag{A.5}$$

and the contour C runs parallel to the z axis. Finally, deforming the contour back to the real axis, we can write the Green's function in terms of the well-known Airy function (see [20] page 447, 10.4.32),

$$\psi(x,t) = \frac{\exp(a_0 t + At)}{(3|a_3|t)^{1/3}}\mathrm{Ai} \times \left\{-\frac{\mathrm{sgn}(a_3)\left(x + \left[a_1 - \frac{a_2^2}{3a_3}\right]t\right)}{(3|a_3|t)^{1/3}}\right\}. \tag{A.6}$$

This is our closed-form expression for the Green's function—note that here we have taken a_3 to be real, but the remaining coefficients may be complex. In what follows we set $a_3 = 1$, as was done earlier in the paper.

The limiting behaviour of the Green's function follows from the well-known asymptotic behaviour of Ai(s) for large $|s|$ (see [20] page 448, 10.4.59, 60):

$$\mathrm{Ai}(s) \sim \frac{\exp(-2s^{3/2}/3)}{2\sqrt{\pi}s^{1/4}} \quad \text{as } s \to \infty \text{ with } |\arg(s)| < \pi,$$
$$\mathrm{Ai}(-s) \sim \frac{\sin\left(\frac{2s^{3/2}}{3} + \frac{\pi}{4}\right)}{\sqrt{\pi}s^{1/4}}$$
$$\text{as } s \to \infty \text{ with } |\arg(s)| < 2\pi/3. \tag{A.7}$$

For fixed t the Green's function decays exponentially as $x \to \infty$ and oscillates and decays algebraically (like $|x|^{-1/4}$) as $x \to -\infty$. The behaviour for large t is more complicated, but can be determined by setting $x = Vt$ and sending $t \to \infty$ with V fixed (for simplicity we now consider the special case of the coefficients a_0, a_1, a_2 being real). We define

$$\chi = \frac{a_2^2}{3} - a_1 - V. \tag{A.8}$$

There are then two separate cases to be considered:

1. If $\chi < 0$ then the Airy function oscillates as $t \to \infty$ (*i.e.* the second asymptotic behaviour in (A.7)), and the stability of the Green's function is determined only by the exponential term $\exp(a_0 t + At)$ in (A.6). It then follows that the Green's function grows exponentially in time if
$$a_2\chi > \frac{a_2^3}{9} - 3a_0. \tag{A.9}$$
2. If $\chi > 0$ then the Airy function decays exponentially as $t \to \infty$ (*i.e.* the first asymptotic behaviour in (A.7)), and the growth or otherwise of the Green's function is then determined by the behaviour of the product of the exponential term $\exp(a_0 t + At)$ and the Airy function in (A.6). After some algebra it follows that the Green's function grows exponentially in time if
$$a_2\chi - \frac{2\chi^{3/2}}{\sqrt{3}} > \frac{a_2^3}{9} - 3a_0. \tag{A.10}$$
This provides a *sufficient* condition for instability when $\chi > 0$, but a necessary condition can be found by noting that the maximum value of the left hand side of (A.10) over all χ is $a_2^3/9$, which occurs when $\chi = a_2^2/3$. This then leads to the *necessary* condition
$$a_0 > 0 \tag{A.11}$$
for instability.

To summarize, the condition for the Green's function to grow exponentially as $t \to \infty$ for a given value of observer velocity V is given by the combination of conditions (A.9) and (A.10). In order to detect the occurrence of absolute instability, we simply need to use conditions (A.9) and (A.10) in the case $V = 0$; when this is done, the results are identical to what is obtained using the standard Briggs–Bers procedure of locating the k pinch point and requiring the imaginary part of the corresponding pinch frequency to be positive.

Finally, we note that the Green's function we have derived is only valid in the case of constant coefficients, and is therefore only relevant to the *local* properties of a spatially inhomogeneous system. Ideally, one would like to be able to determine the Green's function in a spatially-varying case so as to analyse *global* behaviour, as was done by [21] for the usual second-order linearized Ginzburg Landau equation with linear and quadratic spatial variation of the criticality parameter. Unfortunately, this has not proved possible to date for our third-order equation.

References

[1] R.J. Briggs, Electron-stream Interaction with Plasmas, M.I.T. Press, Cambridge, Mass., 1964.
[2] A. Bers, Space–time evolution of plasma instabilities — absolute and convective, in: M.N. Rosenbluth, R.Z. Sagdeev) (Eds.), Handbook of Plasma Physics, North–Holland, Amsterdam, 1983, pp. 451–517.
[3] P. Huerre, P.A. Monkewitz, Absolute and convective instabilities in free shear layers, J. Fluid Mech. 159 (1985) 151–168.
[4] P.A. Monkewitz, K.D. Sohn, Absolute instability of hot jets, AIAA J. 26 (1988) 911–916.
[5] R.J. Lingwood, Absolute instability of the boundary layer on a rotating disk, J. Fluid Mech. 299 (1995) 17–33.
[6] R.J. Lingwood, An experimental study of absolute instability of the rotating-disk boundary-layer flow, J. Fluid Mech. 314 (1996) 373–405.
[7] W. Koch, Local instability characteristics and frequency determination on self-excited wake flows, J. Sound Vib. 99 (1985) 53–83.
[8] P.A. Monkewitz, P. Huerre, J.-M. Chomaz, Global linear stability analysis of weakly non-parallel shear flows, J. Fluid Mech. 251 (1993) 1–20.
[9] P. Huerre, P.A. Monkewitz, Local and global instabilities in spatially developing flows, Annu. Rev. Fluid Mech. 22 (1990) 473–537.
[10] J.-M. Chomaz, P. Huerre, L.G. Redekopp, A frequency selection criterion in spatially developing flows, Stud. Appl. Math. 84 (1991) 119–144.
[11] B.M. Woodley, N. Peake, Global linear stability analysis of thin aerofoil wakes, J. Fluid Mech. 339 (1997) 239–260.
[12] B. Pier, On the frequency selection of finite-amplitude vortex shedding in the cylinder wake, J. Fluid Mech. 458 (2002) 407–417.
[13] S. Le Dizès, P. Huerre, J.-M. Chomaz, P.A. Monkewitz, Linear global modes in spatially developing media, Phil. Trans. R. Soc. Lond. A 354 (1996) 169–212.
[14] B. Pier, P. Huerre, Nonlinear synchronization in open flows, J. Fluids Struct. 15 (2001) 471–480.
[15] J.J. Healey, On the relation between the viscous and inviscid absolute instabilities of the rotating-disk boundary layer, J. Fluid Mech. 511 (2004) 179–199.
[16] C. Leclercq, B. Pier, J. Scott, Absolute instabilities in eccentric Taylor–Couette–Poiseuille flow, J. Fluid Mech. 741 (2014) 543–566.
[17] C.M. Bender, S.A. Orszag, Advanced Mathematical Methods for Scientists and Engineers, McGraw-Hill, New York, 1978.
[18] B. Pier, Signalling problem in absolutely unstable systems, Theor. Comput. Fluid Dyn. 25 (2011) 7–17.
[19] B. Pier, P. Huerre, J.-M. Chomaz, Bifurcation to fully nonlinear synchronized structures in slowly varying media, Physica D 148 (2001) 49–96.
[20] M. Abramowitz, I. Stegun, Handbook of Mathematical Functions, Dover, 1965.
[21] R.E. Hunt, D.G. Crighton, Instability of flows in spatially developing media, Proc. R. Soc. Lond. A 435 (1991) 109–128.